J. Fluid Mech. (1992), *vol.* 239, *pp.* 81–98
Printed in Great Britain

The influence of higher harmonics on vortex pairing in an axisymmetric mixing layer

By R. A. PETERSEN† AND R. C. CLOUGH‡
Department of Aerospace and Mechanical Engineering, University of Arizona, Tucson, AZ 85721

(Received 2 February 1990 and in revised form 22 November 1991)

Strong forcing was used to produce vortex pairing in a submerged axisymmetric water jet. Phase-averaged hot-wire measurements were combined with phase-averaged flow visualization to identify the relevant nonlinear interactions. The leading resonant interaction was not a subharmonic resonance. Instead it was a triad resonance involving the subharmonic, the fundamental and the $\frac{3}{2}$ harmonic. The profound influence of higher harmonics on the amplification of the fundamental and subharmonic was demonstrated in a systematic way by successive truncation of the Fourier series representation of the excitation waveform.

1. Introduction

Historically, ideas about large-scale motion in turbulent, free shear flows have been based on flow visualization. Vorticity is the flow quantity most related to the streakline or dye patterns observed in the visualizations and for that reason the dynamics of the large-scale turbulence originally was modelled kinematically in terms of vortex induction (Brown & Roshko 1974; Winant & Browand 1974). The concept of vortex pairing was introduced by Winant & Browand as the nonlinear mechanism whereby turbulent energy is transferred to larger scales and the shear layer is caused to spread.

Recent studies have shown that linear stability theory is sufficient to describe accurately many features of fully turbulent, free shear flows (Wygnanski & Petersen 1987). The major constraints are (i) the stability theory must be applied to the measured mean velocity profile rather than some model profile and (ii) the divergence of the base flow must be included in the linearized equations. Cross-stream distributions of phase-averaged quantities as well as dispersion relations often can be predicted in this way from stability eigensolutions.

When the mixing layer is axisymmetric, stability solutions are functions of two non-dimensional parameters: reduced frequency $2\pi f\theta/U_j$; and the ratio of shear layer thickness to jet diameter θ/D. The quantities f, θ, U_j, and D refer to wave frequency, mixing-layer momentum thickness, jet speed, and nozzle diameter respectively. The influence of momentum thickness on the stability solutions becomes more pronounced with increasing streamwise distance. However, cross-stream distributions and wavelengths of dominant axisymmetric instabilities including the preferred mode can be predicted from stability theory (Peterson & Samet 1988;

† Present address: Jet Propulsion Laboratory, Pasadena, CA 91109, USA.
‡ Present address: Rocketdyne Division, Rockwell International, Canoga Park, CA 91304, USA.

Samet & Petersen 1988). In this sense there is no generic difference between short-wavelength instabilities dominant near the nozzle exit and the 'preferred mode', dominant near the end of the potential core. In fact at each streamwise location along an unforced jet there was a different 'preferred mode' corresponding to the most amplified instability at that location (Petersen & Samet 1988). This selection process is a consequence of the spreading of the mixing layer.

Both direct and indirect nonlinear interactions are possible when several instabilities with different wavenumbers are present simultaneously. At any given streamwise location the dominant instabilities can contribute to the thickening of the mean velocity profile by means of wave-induced Reynolds stress. The resultant thickening of the mixing layer causes increased amplification of lower-wavenumber instabilities. This indirect exchange of energy from higher to lower wavenumber can be treated within the framework of linear stability theory by specifying the divergent base flow. Direct interactions are quadratic in wave amplitude and can be modelled in terms of triad resonances. The conditions for resonance depend on dispersion relations for the mixing layer which can be modelled from stability eigenvalues.

Both direct and indirect interactions may be involved in vortex pairings. Many of the visual features of a vortex pairing are associated with the linear amplification of a subharmonic wavetrain travelling in a diverging base flow. Stability eigenfunctions exhibit a double peak in the vorticity distribution and mean flow divergence causes the orientation of the double peak to rotate as the wave approaches the point of neutral stability (Michalke 1965; Wygnanski & Weisbrot 1988).

Direct interactions associated with vortex pairings are often modelled in terms of a subharmonic resonance between two wavetrains whose frequency and wavenumber differ by a factor of two. This idealization can be carried over into experimental investigations by exciting the jet with two wavetrains an octave apart in frequency. However, more complicated interactions are possible and direct observations of vortex pairings in unforced flows suggest that the interactions are fundamentally broadband. Pairings are intermittant and often involve more than two vortices (Winant & Browand 1974; Ho & Huang 1982).

The present study is concerned with controlled vortex pairings in an axisymmetric mixing layer. The external excitation was periodic but broadband in frequency. Under broadband excitation the subharmonic resonance is not the dominant interaction. The importance of the higher harmonics to both direct and indirect interactions will be demonstrated in a systematic way by successive truncation of the Fourier series representation of the excitation waveform.

2. Experimental technique

A horizontal, submerged water jet and a vertical air jet were used in this investigation. Both jets used a nozzle exit diameter of 5.08 cm and were designed to operate at the same unit Reynolds number. The details of the water jet were described by Clough (1989) and the air jet was described by Petersen & Samet (1988).

2.1. *Water jet facility*

The water jet is a closed return facility consisting of a plenum, a nozzle based on a fifth-order polynomial, a 1320 l tank, a 61 cm diameter contraction to catch the jet, and a speed-controlled, centrifugal pump. The jet was operated at 50 cm/s which corresponds to a Reynolds number of 2.5×10^4. The centreline turbulence level in the nozzle exit plane was 0.7%.

The large-scale, turbulent motion was controlled mechanically with a Scotch yoke mechanism by periodically constricting the tube supplying the plenum. The peak amplitude of the velocity fluctuation introduced by the scotch yoke mechanism, measured on the jet centreline at the exit plane of the nozzle, was 11% of the jet speed. Because of the large amplitude of the initial disturbance the mechanism of linear amplification may have been bypassed. For this reason the response of the water jet properly can be called a 'forced' response.

Following Winant & Browand (1974) vortical fluid was marked by introducing dye directly into the boundary layer of the nozzle. Strobe illumination, located on the opposite side of the jet from the camera, was used to project an image of the dye onto a mylar sheet on the front side of the tank. The strobe was phase locked to the forcing mechanism and each photograph consisted of an ensemble of 100 strobe flashes.

Phase-averaged measurements of the streamwise component of velocity were made using a single hot-film probe mounted on a computer-controlled traversing mechanism. The maximum calibration drift was 3% over the rather extended sampling durations necessary to obtain accurate statistics.

2.2. *Air jet facility*

The air jet consists of a speed-controlled centrifugal blower, a folded plenum section, and a nozzle based on two tangent arcs. This jet was operated at 16 m/s which resulted in a Reynolds number of 5.4×10^4 based on exit conditions. The jet speed was controlled within 1% and the centreline turbulence level in the nozzle exit plane was 0.15% over 10–10^4 Hz, the frequency range of interest.

The large-scale turbulence was controlled acoustically using a single speaker mounted in the plenum section. The speaker was driven from a digital to analog converter under program control. The peak amplitude of the acoustic disturbance, measured near the jet centreline in the exit plane of the jet nozzle, was 0.13% of the jet speed. This small initial disturbance was intended to excite natural flow instabilities. The response of the flow will be called an 'excited' response to distinguish it from the strong forcing used with the water jet. The fundamental frequency was 125 Hz and the corresponding Strouhal number fD/U_j was 0.40. The jet speed and excitation frequency were selected to match the frequency of the unforced spectral peak at x/D of 4.0 while avoiding acoustic modes of the plenum chamber.

The instrumentation consisted of a ring of eight hot-wire probes equally spaced in polar angle and capable of measuring the streamwise component of velocity. A computer-controlled stepper motor was used to simultaneously traverse all eight wires in the radial direction. The radial traverse extended from a radius of 1.0 cm to the radial location where the mean velocity was 10% of the centreline value. Calibration error was less than 1% including drift and data scatter.

2.3. *Data processing techniques*

The response of the jet to imposed excitations was measured in terms of spatial distributions of phase-averaged quantities. The basic signal processing techniques are described in this section.

Field quantities are expressed in cylindrical coordinates (x, r, ϕ), where r is the polar radius relative to the jet centreline, ϕ is the polar angle and x is the streamwise distance from the nozzle exit plane. The hot wires and the hot film were calibrated *in situ* using plenum pressure as the standard. Sensor voltages were digitized and converted to streamwise component of velocity using a calibration polynomial.

Streamwise velocity can be decomposed into a time-average component, a phase-averaged fluctuation, and a phase-incoherent fluctuation (Hussain & Reynolds 1970):

$$u = U + \hat{u} + u', \tag{2.1}$$

where $\hat{u} = \langle u \rangle - U$ and $u' = u - \langle u \rangle$. Phase-averaged velocity $\langle u \rangle$ is defined

$$\langle u(x, r, \phi, t) \rangle = \frac{1}{N} \sum_{n=1}^{N} u(x, r, \phi, t + t_n), \tag{2.2}$$

where the time reference t_n for the phase-averaged measurements was based on the excitation signal. Slope and level were used as the sampling condition and a latching algorithm was used to prevent multiple triggers in case of noise. The time resolutions were $\frac{1}{128}$ and $\frac{1}{64}$ of the excitation period in the case of the water jet and air jet respectively. The sample size N was generally about 500. The standard deviation of the mean was generally less than 1%.

The phase-averaged velocity was uniform in ϕ and periodic in t. It can be decomposed into a Fourier series with coefficients F_n defined

$$F_n(x, r) = \frac{1}{\pi T} \int_0^{2\pi} \int_0^T \langle u(x, r, \phi, t) \rangle \, \mathrm{e}^{\mathrm{i}2\pi n t/T} \, \mathrm{d}\phi \, \mathrm{d}t. \tag{2.3}$$

Note that F_n is complex and the modulus $|F_n|$ is the local amplitude of the nth harmonic, where $n = 1$ refers to the fundamental.

Vorticity is the feature of large-scale turbulence that is generally emphasized. It is the field quantity that is most closely linked to dye and streakline flow visualizations. It is possible to reconstruct phase-averaged vorticity from single-wire data because of the symmetry and spatial filtering inherent in phase-averaged measurements. Using continuity the phase-averaged vorticity component $\langle \omega_\phi \rangle$ can be determined from the following equation:

$$\langle \omega_\phi \rangle = -\frac{\partial}{\partial r} \langle u \rangle - \frac{1}{r} \int_0^r r' \frac{\partial^2}{\partial x^2} \langle u \rangle \, \mathrm{d}r'. \tag{2.4}$$

Because of the boundary-layer nature of the phase-averaged flow the second term in (2.4), which has the greatest potential for error, was generally less than a tenth the size of the first term.

The measurement locations were equally spaced at eighth-wavelength intervals in the streamwise direction. The radial profiles were interpolated to produce data equally spaced at $0.02D$ intervals in radius. First and second derivatives were calculated numerically using 5-point smoothing. The smoothing 'cutoff' frequency was designed to be about half the Nyquist bandwidth. Consequently the spatial resolution was roughly a half-wave for streamwise derivatives and $0.08D$ for radial derivatives.

The algorithm is validated in figure 1 by applying it to numerical 'data' generated analytically from a stream function. The stream function

$$\psi(x, y) = \tfrac{1}{2}y - \theta \ln\left[\cosh\left(\frac{y - 0.5}{2\theta}\right) - \rho \cos(2\pi x)\right], \quad y > 0 \tag{2.5}$$

is based on a steady-state solution for a plane mixing layer discovered by Stuart (1967). In the present context it is a model for a planar half-jet. The analytic vorticity $\nabla^2\psi$ is shown in figure 1 (*a*) where values of θ and ρ were selected to be 0.08

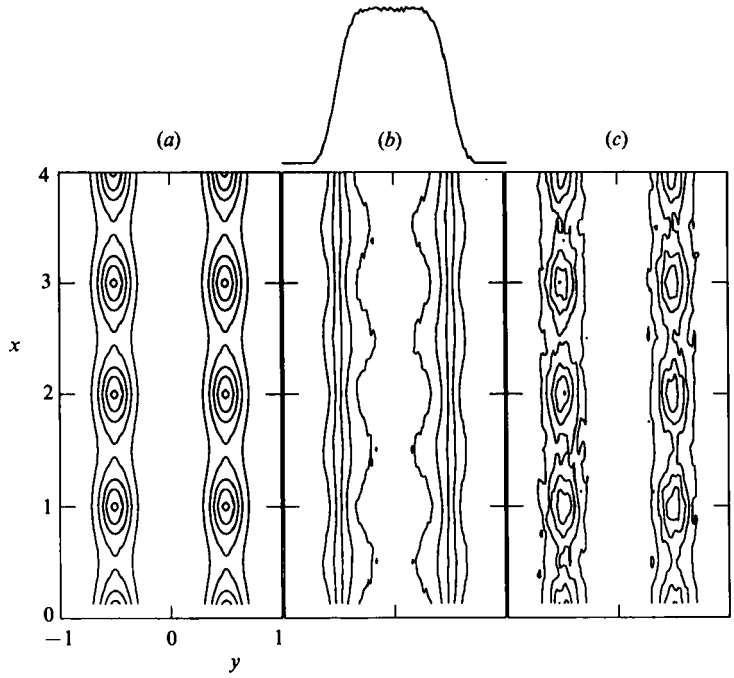

FIGURE 1. Vorticity reconstruction from numerical 'data'. (*a*) Vorticity, $\omega = -\nabla^2\psi$; (*b*) streamwise velocity, $u = \partial\psi/\partial y + 1\%$ random noise; (*c*) reconstruction based on equation (2.4) in rectangular coordinates.

and 0.25. The analytic velocity $\partial\psi/\partial y$ is shown in figure 1 (*b*). Uniformly distributed random numbers have been superimposed to simulate statistical uncertainty. The standard deviation of the random numbers is 1%. This represents an upper limit to the statistical uncertainty of the phase-averaged measurements. The vorticity reconstruction is shown in figure 1 (*c*). It was obtained by applying a rectangular coordinate version of (2.4) to the 'data' of figure 1 (*b*). The location and levels of the vorticity maxima of figure 1 (*a*) were reconstructed with reasonable accuracy in figure 1 (*c*). In the absence of synthetic noise the reconstruction was virtually identical to figure 1 (*a*).

3. The vortex pairing

The water jet was forced at 3 Hz using the Scotch yoke mechanism. This was the frequency of the 'preferred mode' dominant at $x/D = 4$ and the corresponding Strouhal number fD/U_j, based on nozzle diameter, was 0.30. At any other location along the potential core the frequency of the most energetic instability was greater than 3 Hz. Because of the large-amplitude, pulsatile nature of the forcing a broadband spectrum of harmonics of 3 Hz were also introduced. These harmonics encompassed the entire range of instabilities dominant at any given location along the potential core.

Phase-averaged dye visualizations and phase-averaged measurements of $\langle u \rangle$ were obtained at identical phase delays relative to the Scotch yoke mechanism. The vorticity reconstruction (2.4) was applied to phase-averaged $\langle u \rangle$ and the results are shown in figure 2. Sections are shown at various phase delays in a plane that includes

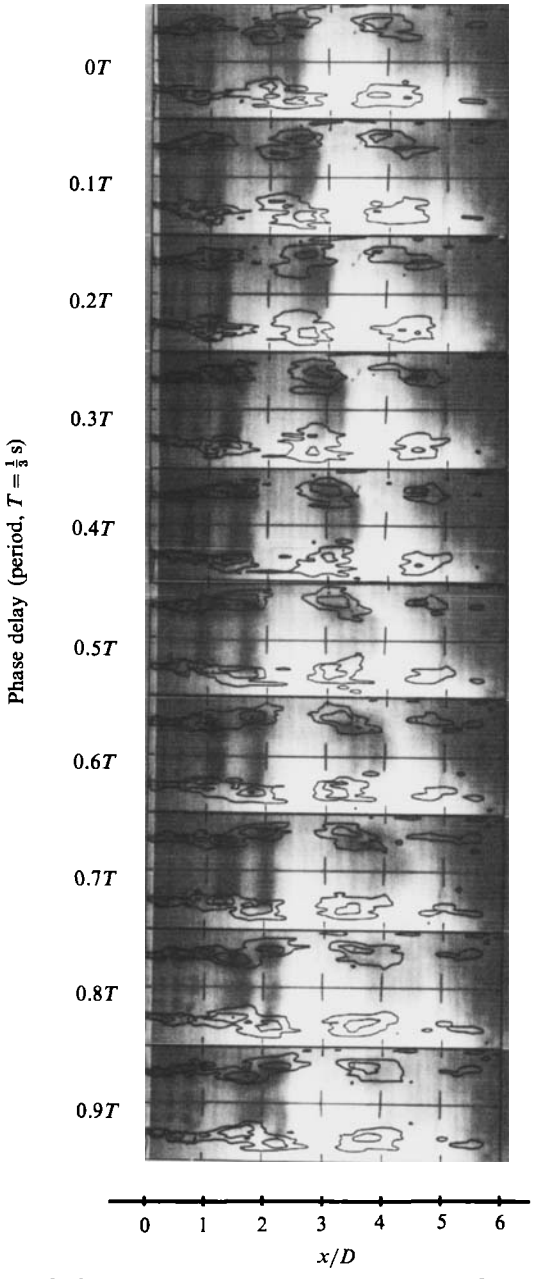

FIGURE 2. Contours of phase-averaged vorticity superimposed on phase-averaged flow visualization. Jet speed: 50 cm/s; nozzle diameter: 5.08 cm; forcing frequency: 3.0 Hz; vorticity contour levels: 15, 30, 60, 120 s^{-1}.

the jet centreline. Contours of phase-averaged vorticity $\langle \omega_\phi \rangle$ are superimposed on the phase-averaged dye visualizations. The dye photographs are averaged over 100 flashes of a strobe light using the technique described in §2.1. The vorticity contour levels are spaced logarithmically to approximate the response of photographic film to light intensity.

Within the range x/D from 1.0 to 3.0 concentrations of dye and vorticity coincided

exactly. Upstream of x/D of 1.0 the spatial resolution of the vorticity reconstruction was insufficient to capture the closely spaced vortex rings. Downstream of x/D of 3.0 the dye concentrations were displaced slightly downstream from the vorticity maxima.

Several vortex amalgamations are evident both from the dye visualizations and from the vorticity contours. A pairing at $x/D = 2.5$ can be identified based on the criterion of cross-stream alignment of the two vortices (Ho & Huang 1982). This pairing involved the lowest-order harmonics of the forcing and in that sense it represents the leading nonlinear interaction. The dye photographs and the vorticity reconstructions show identical patterns of acceleration and eventual amalgamation of the upstream ring with the downstream ring. Downstream from the pairing the passage frequency of the vortex rings was 3 Hz, the frequency of excitation. Upstream of the pairing the passage frequency was 6 Hz, the first harmonic of the forcing. Even though the frequency of most energetic spectral peak had shifted by an octave, the vortex pairing shown in figure 2 was not a subharmonic resonance. This will be established in a variety of ways.

Figure 3 is a one-dimensional space–time diagram depicting trajectories of individual vortex rings. It was produced by tracking the dye concentrations from figure 2. The vortex pairing was in reality a complicated amalgamation involving as many as seven individual vortex rings. The pattern of vortex trajectories is periodic on a 3 Hz cycle but not on a 6 Hz cycle. Consequently, the amalgamations were not a series of binary pairings.

The Scotch yoke mechanism produced a periodic series of pulses containing a spectrum of harmonics. The linear amplification of the various harmonics is a function of the shear-layer thickness. For present purposes the shear-layer momentum thickness is defined

$$\theta_{0.1} = \int_0^{R_{0.1}} \frac{U(r)}{U_0}\left[1-\frac{U(r)}{U_0}\right]\mathrm{d}r, \tag{3.1}$$

where U_0 is the local centreline velocity and $R_{0.1}$ is the radial location where $U/U_0 = 0.1$. Integral (3.1) was truncated to avoid the outer edge of the jet where hot-wire measurements are known to be inaccurate. Solutions of the stability equations are functions of reduced frequency $2\pi f\theta_{0.1}/U_j$ and ratio of shear-layer thickness to jet diameter $\theta_{0.1}/D$ (Michalke 1971).

Power spectral densities of streamwise velocity are shown in figure 4 plotted against frequency and against reduced frequency. The measurements were made at the inside edge of the mixing layer along a ray extending from the nozzle lip to the jet centreline at $x/D = 4$. At each location the forced spectrum is superimposed on the unforced spectrum. There is an obvious shift of the spectral peaks in figure 4(*a*) to lower frequency with increasing streamwise distance. The unforced spectral peak shifted from 24 to 3 Hz over the x/D range from 0.25 to 4. The most energetic harmonics in the forced spectra tracked the unforced spectra, shifting from 15 to 3 Hz over the same range of x/D.

Features of figure 4 can be explained qualitatively within the framework of linear theory. At each x/D the most energetic spectral peak, figure 4(*b*), fell within the range of reduced frequency 0.12–0.34. These values are consistent with the band of unstable waves predicted from linear stability theory. The reduced frequency of a neutrally amplified wave usually falls between 0.3 and 0.4, depending on the shape of the mean velocity profile (Petersen & Samet 1988). A wave with that frequency

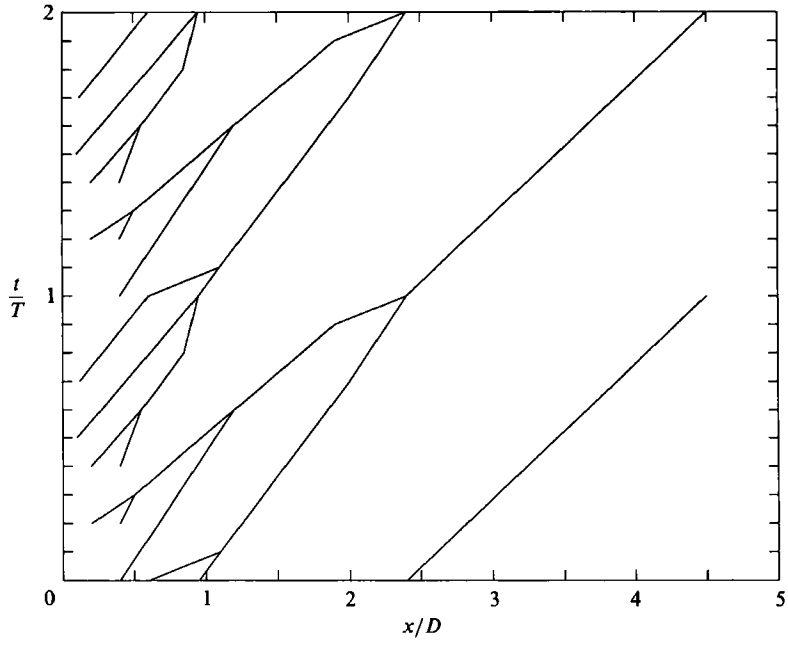

FIGURE 3. Space–time trajectories of dye concentrations from figure 2.

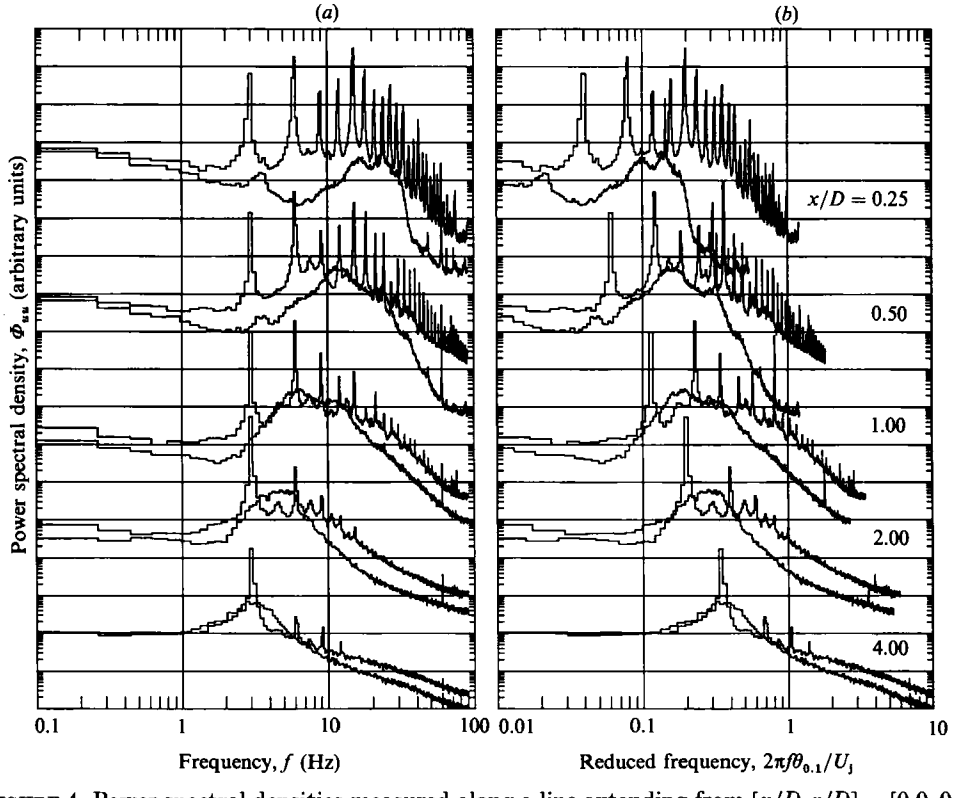

FIGURE 4. Power spectral densities measured along a line extending from $[x/D, r/D] = [0.0, 0.5]$ to $[4.0, 0.0]$. Forced and unforced spectra superimposed at each streamwise location. Frequency scale: (*a*) dimensional; (*b*) normalized by local shear-layer thickness.

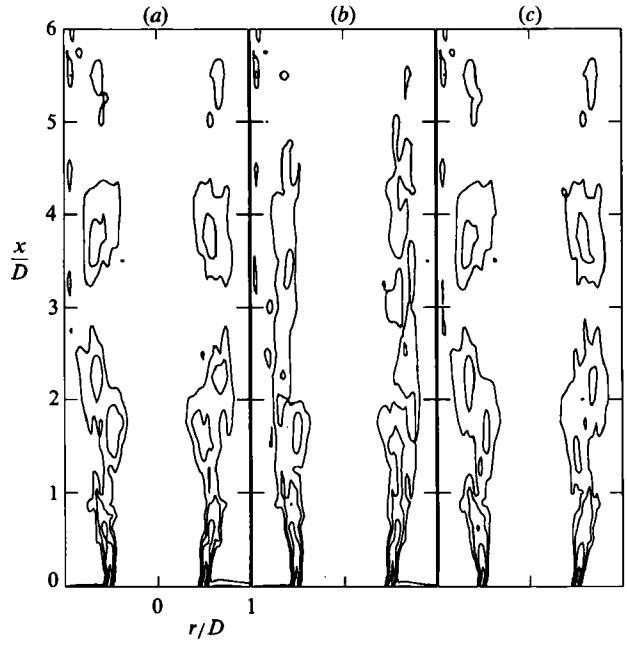

FIGURE 5. Narrowband vorticity reconstructions. Spectral content (*a*) 3 Hz + 6 Hz + 9 Hz; (*b*) 6 Hz + 9 Hz; (*c*) 3 Hz. Time delay: $t/T = 0.9$; contour levels same as figure 2.

will have experienced its maximum cumulative amplification. Waves with higher frequency will be exponentially damped.

Within the framework of the previous, linear arguments there are nonlinear mechanisms implicit in the spreading of the mean flow. The underlying nonlinearities include momentum transfer to the mean flow through wave-induced stresses. The uppermost spectra in figure 4 provide an example. At $x/D = 0.25$ the frequency of the most energetic forced harmonic was less than the frequency of the natural instability (figure 4*a*). However, the corresponding reduced frequency was larger (figure 4*b*). This is a consequence of changes in the shape of the mean velocity profile caused by the forced unsteady flow.

Linear arguments can also be applied to vortex amalgamations. Many of the visual features of a vortex pairing can be explained in terms of the linear saturation of a subharmonic wave in a diverging base flow (Wygnanski & Weisbrot 1988, figures 1 and 2). In figure 5, following Wygnanski & Weisbrot, vorticity contours (figure 5*a*) were filtered to extract (i) the fundamental plus $\frac{3}{2}$ harmonic (figure 5*b*) and (ii) the subharmonic alone (figure 5*c*). The double-peak structure in the vorticity distribution was associated more with the subharmonic (compare figures 5 (*a* and *c*)) than with the fundamental. Filtering at the higher harmonics captured only the upstream vorticity peak (compare figure 5 (*a* and *b*)). As a consequence the double peak structure in the vorticity distribution and the merging process alone are insufficient evidence of direct, nonlinear energy transfer between waves.

In the case of a plane mixing layer, the location of vortex pairing coincides with the saturation of the subharmonic (Ho & Huang 1982). For the pairing shown in figure 5 the frequency of the subharmonic was 3 Hz, the forcing frequency. The frequency of the fundamental was 6 Hz. The actual location of the pairing, based on cross-stream alignment of the two vortices, was $x/D = 2.5$ (figure 2). The streamwise

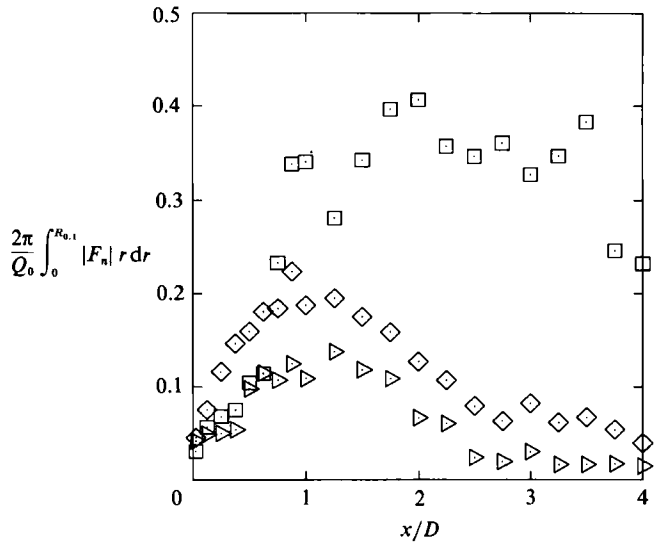

FIGURE 6. Streamwise distribution of phase-averaged modulus integrated across the shear layer and normalized by exit conditions: ⊡, 3 Hz subharmonic; ◇, 6 Hz fundamental ▷, 9 Hz harmonic.

distribution of subharmonic amplitude is shown in figure 6 along with the fundamental and $\frac{3}{2}$ harmonic. The amplitude is expressed as the phase-averaged modulus integrated across the mixing layer:

$$\frac{2\pi}{Q_0}\int_0^{R_{0.1}} |F_n|\, r\, dr. \tag{3.2}$$

The modulus $|F_n|$ was obtained from phase-averaged hot-wire measurements using (2.3). The normalization is based on the initial volume flux Q_0 at the nozzle exit plane. Based on this measure, the subharmonic saturated at $x/D = 2.0$, slightly upstream of the pairing location. The peaks in the distributions of subharmonic and fundamental each occurred one wavelength from the nozzle. This rapid amplification and the rather high levels are consequences of the strong forcing.

The prediction of total amplification, as in figure 6, is one area where linear theory generally fails. Even when non-parallel terms are retained the linear theory predicts amplitudes that are considerably larger than measured (e.g. Wygnanski & Petersen 1987, figure 5). That is because total amplification is particularly sensitive to energy transfer to other waves by direct nonlinear interactions.

In the present case the leading, direct nonlinear interaction associated with the vortex pairing shown in figures 2 and 5 is not a subharmonic resonance. By examining the relative phase advance of the lowest-order harmonics it will be shown that the leading interaction involves the 3 Hz subharmonic, the 6 Hz fundamental and the $\frac{3}{2}$ harmonic.

The phase advance of a wavetrain propagating through a two-dimensional, dispersive shear layer can be expressed as (Crighton & Gaster 1976)

$$\Psi_n(x,\eta) = \psi_n(x_0,\eta) + \int_{x_0}^{x} \alpha_n(\xi,\eta)\, d\xi. \tag{3.3}$$

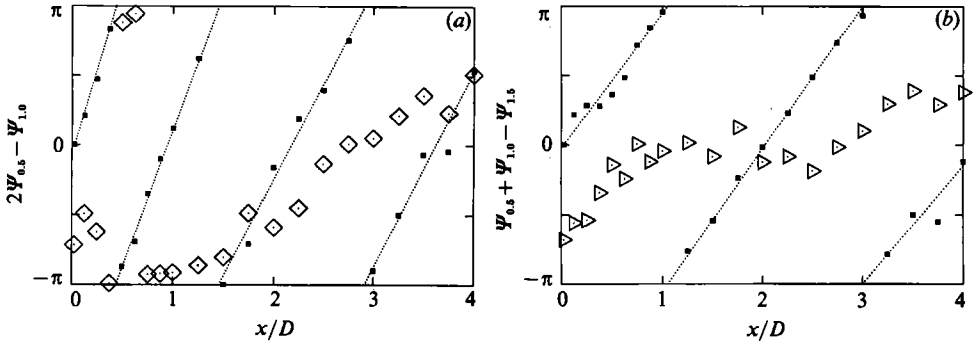

FIGURE 7. Streamwise distribution along $\eta = -3.5$ of phase difference appropriate to (*a*) subharmonic resonance and (*b*) triad resonance between subharmonic, fundamental and $\frac{3}{2}$ harmonic. —■—, Phase advance of (*a*) 6 Hz fundamental and (*b*) 3 Hz subharmonic shown for reference.

The subscript n refers to the harmonic number, α_n is the streamwise wavenumber, $\psi_n(x_0, \eta)$ is the initial phase offset, and η is the radial similarity coordinate defined

$$\eta = [r - R_{0.5}]/\theta_{0.1}. \tag{3.4}$$

Because the leading nonlinearity in the momentum equation is quadratic in disturbance amplitude, the leading resonant interaction will involve a triad of waves. In order for a particular triad resonance to occur the resonance conditions must be compatible with the dispersion relationship for the waves. The resonance conditions for a subharmonic resonance between a wavetrain with fundamental frequency and two wavetrains with subharmonic frequency are (Phillips 1974)

$$f_1 = 2f_{0.5}; \quad \alpha_1 = 2\alpha_{0.5}, \tag{3.5}$$

where the subscripts $n = 0.5$ and $n = 1$ refer to the subharmonic and fundamental respectively.

The possibility of a subharmonic resonance can be tested by examining the phase difference $\Psi_{0.5} - \Psi_1$. From (3.3) and along a path of constant η:

$$2\Psi_{0.5}(x) - \Psi_1(x) = 2\psi_{0.5} - \psi_1 + \int_{x_0}^{x} [2\alpha_{0.5}(\xi) - \alpha_1(\xi)]\, \mathrm{d}\xi. \tag{3.6}$$

If there is a subharmonic resonance then from (3.5) the integrand should vanish and according to (3.6) the phase difference $2\Psi_{0.5} - \Psi_1$ ought to be constant with x, the streamwise distance.

In practice Ψ_n is the phase of F_n calculated from phase-averaged hot-wire measurements according to (2.3). The subharmonic resonance hypothesis was tested using measured phase angles and the results are shown in figure 7 (*a*). The phase angles were measured along $\eta = -3.5$ which is located inside the potential core near the edge of the mixing layer. The phase difference was not constant with x. By implication the subharmonic resonance conditions (3.5) were not satisfied. At the location of the pairing, $x/D = 2.5$, the slope was positive. From (3.6) a positive slope implies $2\alpha_{0.5} > \alpha_1$, which implies that the phase speed of the fundamental $2\pi f_1/\alpha_1$ exceeded $\pi f_1/\alpha_{0.5}$, the phase speed of the subharmonic. Based on the phase advance of the fundamental, shown in figure 7 (*a*) for reference, the average wavelength λ/D of the 6 Hz fundamental was 1.2 and the average phase speed c/U_j was 0.73.

Next we consider the triad resonance involving the subharmonic, the fundamental and the $\frac{3}{2}$ harmonic. The resonance conditions are

$$f_{1.5} = f_{0.5} + f_1; \quad \alpha_{1.5} = \alpha_{0.5} + \alpha_1. \tag{3.7}$$

The frequency of the $\frac{3}{2}$ harmonic was 9 Hz, the second harmonic of the forcing frequency. The existence of this resonance can be verified by examining the phase difference $\Psi_{0.5} + \Psi_1 - \Psi_{1.5}$. From (3.3) and along a path of constant η:

$$\Psi_{0.5}(x) + \Psi_1(x) - \Psi_{1.5}(x) = \psi_{0.5} + \psi_1 - \psi_{1.5} + \int_{x_0}^{x} [\alpha_{0.5}(\xi) + \alpha_1(\xi) - \alpha_{1.5}(\xi)]\, \mathrm{d}\xi. \tag{3.8}$$

If the resonance conditions (3.7) are satisfied then the integrand will vanish and the phase difference (3.8) should be constant with x.

The triad hypothesis (3.7) was tested by measuring the phase difference $\Psi_{0.5} + \Psi_1 - \Psi_{1.5}$. The results, shown in figure 7 (*b*), are consistent with the hypothesis. From approximately $x/D = 0.5$ to approximately $x/D = 2.5$ the phase difference was constant within the scatter of the data. The streamwise region extends one subharmonic wavelength and includes the location of the vortex pairing. Based on the phase advance of the 3 Hz subharmonic, included in figure 7 (*b*) for reference, the average wavelength λ/D of the subharmonic was 2.1 and the average phase speed c/U_j was 0.64.

4. Forcing with controlled waveform

In this section we will describe measurements made in the air jet facility using computer-controlled, acoustic excitation. It will be shown that the principal conclusions from the water jet measurements of the previous section were verified using the air jet facility which operated at a higher Reynolds number and at a much lower excitation level. In addition the acoustic excitation enabled much greater control over the excitation waveform than was possible with the scotch yoke mechanism used with the water jet. Control over the waveform allowed a direct comparison between broadband excitation and a true subharmonic resonance. Also, the effects of higher harmonics were investigated in a systematic way by successively truncating the Fourier series representation of the basic waveform.

A 'sawtooth' wave was selected as the basic excitation waveform. A single period of the sawtooth is defined by the following expression:

$$2A\left[\frac{1}{2} - \frac{t}{T}\right], \tag{4.1}$$

where A is the wave amplitude and T is the period. The sawtooth wave simulates a periodic series of impulses and was intended as a rough approximation to the waveform produced by the scotch yoke mechanism.

A subharmonic resonance was created by truncating the Fourier series expansion of (4.1) at the two lowest harmonics. The resulting expression is

$$\frac{2A}{\pi}\left[\sin\left(\frac{2\pi t}{T}\right) + \tfrac{1}{2}\sin\left(\frac{4\pi t}{T}\right)\right]. \tag{4.2}$$

In accordance with the water jet experiment, the period T was selected such that the base frequency $f = 1/T$ matched the 'preferred mode' at x/D of 4. For the air jet the

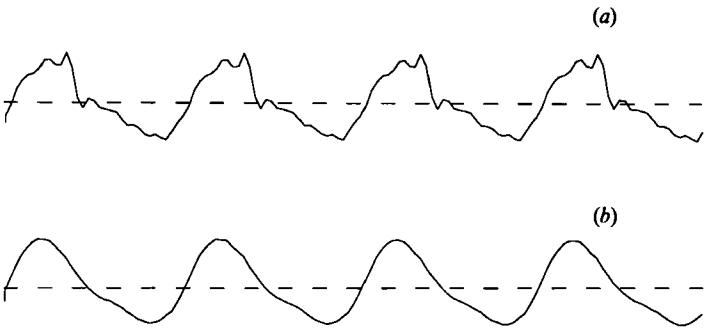

FIGURE 8. Phase-averaged acoustic waveforms corresponding to excitation by (*a*) a sawtooth wave, equation (4.1), and (*b*) the two-term truncation, equation (4.2). Acoustic amplitudes: 2.0 cm/s; measurement location: $[x/D, r/D] = [0.25, 0.20]$.

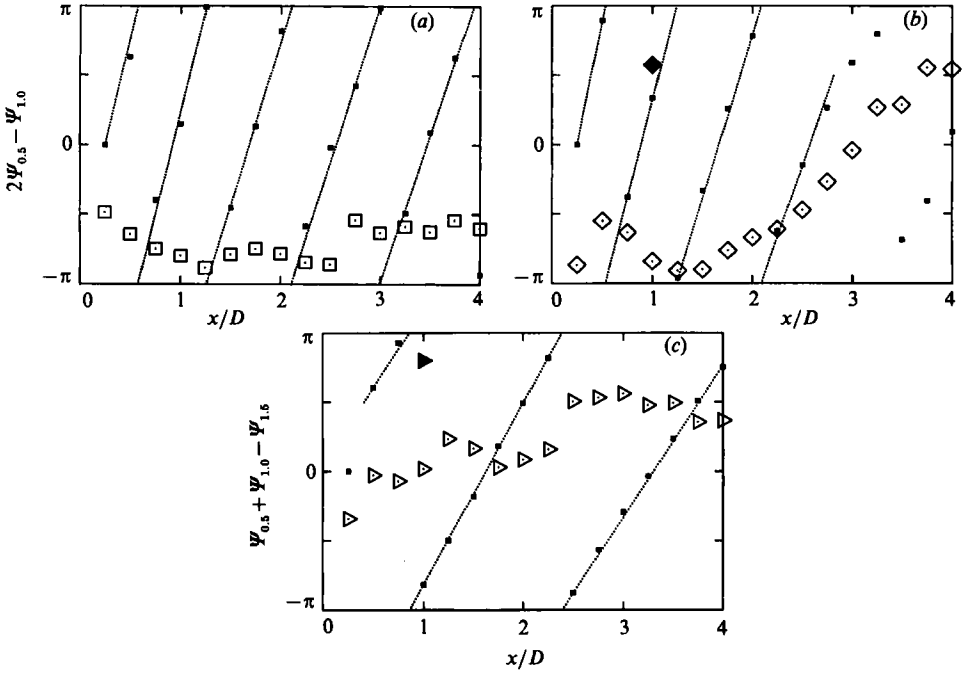

FIGURE 9. Streamwise distribution along $\eta = -2.6$ of phase difference appropriate to subharmonic resonance in the case of excitation with: (*a*) two-term truncation; (*b*) sawtooth wave; and (*c*) phase difference appropriate to triad resonance between subharmonic, fundamental and $\frac{3}{2}$ harmonic in the case of a sawtooth excitation. Solid symbols refer to sawtooth excitation but with reversed sign. Phase advance of (*a*, *b*) 250 Hz fundamental and (*c*) 125 Hz subharmonic shown for reference.

base frequency was 125 Hz and the corresponding Strouhal number fD/U_j was 0.397. Waveform (4.2) can be viewed as a 125 Hz 'subharmonic' superimposed on a weaker 250 Hz 'fundamental'. Excitation using this waveform provided a reference for evaluating the response of the jet to the sawtooth wave.

The measured acoustic waveforms (4.1) and (4.2) are shown in figure 8. They were measured using a hot wire located near the centreline, nozzle exit plane. The jet was operated at low speed, 1.3 m/s, sufficient to provide a polarizing flow. The sawtooth waveform (4.1) had been modified to include a $0.1T$ rise time to accommodate the response of the plenum speaker. This resulted in a more rapid roll-off of the higher

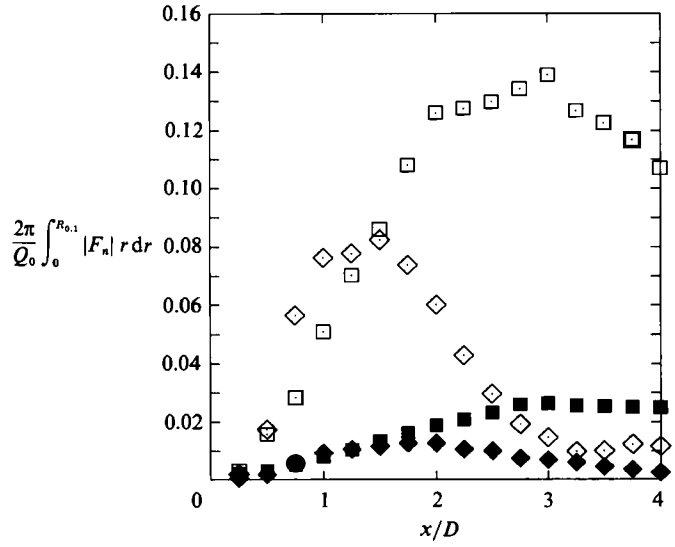

FIGURE 10. Streamwise distribution of phase-averaged modulus: ⊡, 125 Hz subharmonic; ◇, 250 Hz fundamental; open symbols, sawtooth excitation; solid symbols; two-term truncation.

harmonics but had minimal impact on the lower harmonics. The acoustic amplitude A (figure 8) was 2.0 cm/s. At the jet operating speed of 16 m/s this amplitude corresponds to an excitation level A/U_j of 0.13%.

The leading resonances are documented in figure 9. The phase differences were measured along $\eta = -2.6$ which corresponds to $U(r)/U_j$ of approximately 0.96. Waveform (4.2) produced a subharmonic resonance as expected. The fundamental and subharmonic waves were phase-locked over most of the potential core region, figure 9(*a*). The sawtooth excitation, figure 9(*b*), did not produce a subharmonic resonance. Instead, the sawtooth excitation produced a triad resonance between the subharmonic, fundamental and $\frac{3}{2}$ harmonic (figure 9*c*). Note the similarity between the phase distributions of figure 9(*b*, *c*) and the distributions shown in figure 7, measured with the water jet.

The nonlinear response was sensitive to the polarity of the sawtooth wave. Symmetry of the response was examined by reversing the sign of the amplitude A in (4.1). The sign reversal resulted in asymmetries in both amplification and phase advance. Reversing the sign ought to introduce a phase shift of $-\pi$ between the fundamental and subharmonic and likewise between the $\frac{3}{2}$ harmonic and the sum of fundamental plus subharmonic. At x/D of 1.0 the measured phase shifts were -0.6π (figure 9*b*) and $+0.8\pi$ (figure 9*c*).

Streamwise distributions of the phase-averaged response are shown in figure 10. Integrated moduli evaluated across the mixing layer are shown for the 125 and 250 Hz spectral components. The moduli were calculated from phase-averaged hot-wire measurements using (2.3). The sawtooth wave and the truncated waveform were introduced at equal amplitude (figure 8). However, the nonlinear response of the jet to the sawtooth was larger by a factor of 5. To place this in perspective, the forced response of the water jet, figure 6, was larger by a factor of 3 than the response of the air jet to sawtooth excitation. However, the level of forcing was larger by a factor of 100.

The rate of amplification per wavelength was smaller for the air jet than the water jet. The peak levels of the integrated moduli occurred two wavelengths from the

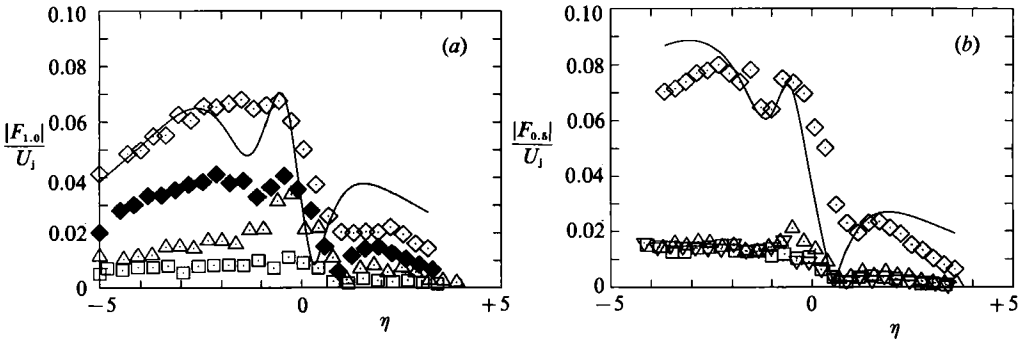

FIGURE 11. Cross-stream distributions of phase-averaged moduli of fundamental $F_{1.0}$ and subharmonic $F_{0.5}$ for various excitation waveforms: ◇, sawtooth excitation; ◆, sawtooth with reversed sign; ⊡, two-term truncation; ▽, three-term truncation; △, four-term equation; ——, stability eigenfunction. Momentum thickness θ calculated from equation (3.1). (*a*) $x/D = 1.0$, $\alpha_{1.0}\,\theta = 0.390—0.053\mathrm{i}$; (*b*) $x/D = 2.0$, $\alpha_{0.5}\,\theta = 0.349-0.044\mathrm{i}$.

nozzle exit as opposed to one wavelength for the distributions shown in figure 6. That is one reason to make a distinction between 'forced' and 'excited' response.

The differences in response to the sawtooth waveform (4.1) as compared to waveform (4.2) were caused by the presence of higher harmonics. The sensitivity to harmonic content was examined by truncating the Fourier series expansion of (4.1) at successively higher harmonics. Some of the results are shown in figure 11. Cross-stream distributions of fundamental and subharmonic modulus are shown for excitation by two-, three- and four-term truncations of the sawtooth wave. The convergence was rather slow. In fact as many as 10 harmonics were required in order to achieve the same response as the sawtooth. The response was sensitive to the initial rise time of the sawtooth; the amplification diminished when the rise time exceeded $0.1T$. The key requirement was that enough terms be retained to include the frequency of the initial shear-layer instability. The overlap between the initial shear-layer instability and higher harmonics of the forcing was observed previously in connection with the water-jet spectral measurements (figure 4, $x/D = 0.25$).

The shapes of the distributions of fundamental and harmonic, figure 11, are not sensitive to the presence of higher harmonics. This would be more apparent if the distributions were scaled to enclose the same area. Eigenfunction moduli calculated from linear, inviscid stability theory are included for comparison (see Peterson & Samet 1988, for computational details). The eigenfunctions were calculated for frequencies of 250 Hz ($x/D = 1.0$) and 125 Hz ($x/D = 2.0$). The two reduced frequencies were both approximately 0.24 and the two waves were still slightly unstable at the two respectively streamwise locations. The eigenfunctions are scaled to the sawtooth distributions and there is rough agreement in the shapes.

Changing the polarity of the sawtooth excitation did not affect the shape of the cross-stream distribution of the fundamental, figure 11. However, the amplification was significantly reduced. This lack of symmetry in the response of the flow is a surprising result and the mechanism is not yet understood.

As a final comment we note a difference between planar and axisymmetric mixing layers in their respective global sensitivity to external excitation. When shear-layer instabilities are excited at sufficiently high levels in a plane mixing layer the saturation of the excited mode can inhibit the growth of the shear layer (Ho & Huang 1982; Weisbrot & Wygnanski 1988). This can result in a plateau or even in an overshoot in the streamwise distribution of shear-layer thickness.

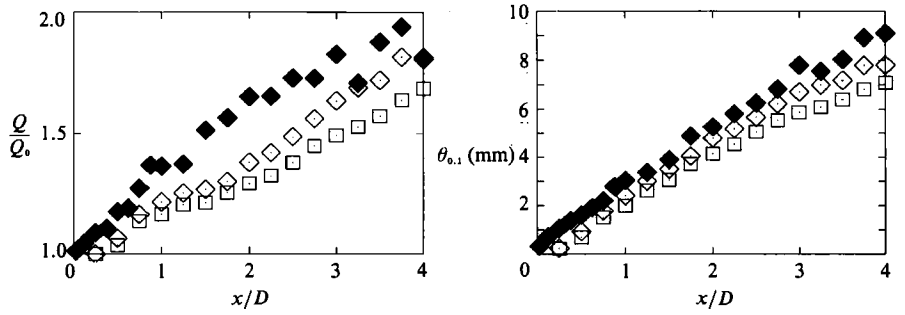

FIGURE 12. Streamwise distribution of volume flux Q/Q_0 and mixing-layer thickness $\theta_{0.1}$: ◆, water jet with 3 Hz forcing; ◇, air jet with sawtooth excitation; ⊡, excitation with two-term truncation.

A similar effect was not observed in the case of the axisymmetric mixing layer. Streamwise distributions of shear-layer thickness $\theta_{0.1}$ and volume flux are shown in figure 12 for various different excitation waveforms and levels. The volume flux Q is defined by the following equation:

$$Q = \frac{1}{2\pi}\int_0^{2\pi}\int_0^{R_{0.1}} U(r,\phi)\, r\, \mathrm{d}r\, \mathrm{d}\phi. \tag{4.3}$$

The normalization Q_0 is the initial 'tophat' volume flux calculated from jet speed and diameter. The integrated flux was underestimated due to the $R_{0.1}$ truncation and Q_0 was overestimated due to the tophat assumption. The combined error of the ratio was about 3%, estimated by extrapolation to the origin. The error would increase with jet spreading because of radial bias but it was not considered to be so large as to obscure trends.

From figure 12 it is apparent that entrainment was enhanced by external excitation or forcing. Natural spreading was identical to excitation with waveform (4.2) and is not shown. At very high levels of forcing the water jet volume flux distribution showed a slight change of slope beyond $x/D = 2$. However, there was not a distinct plateau. The effect on momentum thickness was modest at all levels of forcing. In particular, truncating the series expansion of the sawtooth wave had only minor effects on the mean flow. This means that the profound differences in amplification, figures 10 and 11, cannot be explained by linear stability arguments.

It should be emphasized that the base frequency of the excitation waveforms was selected to match the most amplified instability near $x/D = 4$. One would expect three-dimensional effects to be more pronounced near the end of the potential core than near the nozzle lip. If the frequency had been selected to excite instabilities nearer the lip then it is possible that the response in that region might have been more like a plane mixing layer.

5. Conclusions

The term 'vortex pairing' was introduced by Winant & Browand (1974) to describe as phenomenon that was fundamentally broadband. Nevertheless, theoretical and numerical treatments usually model a vortex pairing by a subharmonic resonance between two monochromatic wavetrains. Laboratory experiments often create the same idealized boundary conditions. In the present study when vortex pairings were produced by broadband excitation the leading interaction was not a subharmonic

resonance. By inference it is possible that subharmonic pairings may not be representative of natural mixing layers.

Periodic, pulsatile waveforms contain a spectrum of harmonics whose power decreases with harmonic number. Experiments were performed in two different jet facilities at two different Reynolds numbers. The jets were forced or excited by two different pulsatile waveforms whose amplitudes differed by a factor of 100. In each case the leading nonlinear interaction was a triad resonance involving the fundamental, the subharmonic and the $\frac{3}{2}$ harmonic.

The importance of the spectrum of higher harmonics was demonstrated by exciting an air jet with a sawtooth wave and then comparing the response with excitation waveforms where the Fourier expansion of the sawtooth was truncated at successively fewer terms. Truncating the sawtooth expansion at the first two terms resulted in a true subharmonic resonance between the two wavetrains. However, the amplification of the base excitation frequency was only 20% as large as when the higher harmonics were retained.

The key requirement was that enough terms be retained to include the frequency of the initial shear-layer instability. We feel that this overlap between the initial shear-layer instability and higher harmonics of the forcing may be similar to the 'collective interaction' concept introduced by Ho & Huang (1982). They observed an interaction between the initial shear-layer instability and a single long-wavelength, high-amplitude wave. In the present case there appears to be a cascade of energy over a spectrum of wavenumbers.

The most significant *direct* nonlinear interaction was a triad resonance between the subharmonic, fundamental and $\frac{3}{2}$ harmonic. However, the most significant nonlinear interactions appear to be indirect. Many visual features of the vortex pairing and the transfer of energy to lower harmonics can be explained qualitatively within the framework of linear theory applied to a divergent mean flow. The mechanisms responsible for the spreading of the mixing layer include wave-induced Reynolds stresses.

This work was supported by the NASA Lewis Research Center under Grant NAG 3-460 and by the National Science Foundation under Grant MSM 8800086.

REFERENCES

Brown, G. L. & Roshko, A. 1974 On density effects and large structure in turbulent mixing layers. *J. Fluid Mech.* **64**, 775–816.

Clough, R. C. 1989 Vortex interactions in an axisymmetric water jet. M.S. dissertation, University of Arizona, Tucson.

Crighton, D. G. & Gaster, M. 1976 Stability of slowly diverging jet flow. *J. Fluid Mech.* **77**, 397–413.

Ho, C. M. & Huang, L. S. 1982 Subharmonics and vortex merging in mixing layers. *J. Fluid Mech.* **119**, 443–473.

Hussain, A. K. M. F. & Reynolds, W. C. 1970 The mechanics of an organized wave in turbulent shear flow. *J. Fluid Mech.* **41**, 241–258.

Michalke, A. 1965 Vortex formation in a free boundary layer according to stability theory. *J. Fluid Mech.* **22**, 371–383.

Michalke, A. 1971 Instabilität eines Kompressiblen runden Freistrahls unter Berücksichtigung des Einflusses der Strahlgrenzschichtdicke. *Z. Flugwiss.* **19**, 319–328.

Petersen, R. A. & Samet, M. M. 1988 On the preferred mode of jet instability. *J. Fluid Mech.* **194**, 153–173.

PHILLIPS, O. M. 1974 Wave interactions. In *Nonlinear Waves* (ed. S. Leibovich & A. R. Seebass), pp. 186–211. Cornell University Press.

SAMET, M. M. & PETERSEN, R. A. 1988 Effects of excitation level on the stability of an axisymmetric mixing layer. *Phys. Fluids* **31**, 3246–3252.

STUART, J. T. 1967 On finite amplitude oscillations in laminar mixing layers. *J. Fluid Mech.* **29**, 417–440.

WEISBROT, I. & WYGNANSKI, I. 1988 On coherent structures in a highly excited mixing layer. *J. Fluid Mech.* **195**, 137–159.

WINANT, C. D. & BROWAND, F. K. 1974 Vortex pairing, the mechanism of turbulent mixing-layer growth at moderate reynolds number. *J. Fluid Mech.* **63**, 237–255.

WYGNANSKI, I. & PETERSEN, R. A. 1987 Coherent motion in excited free shear flows. *AIAA J.* **25**, 201–213.

WYGNANSKI, I. & WEISBROT, I. 1988 On the pairing process in an excited plane turbulent mixing layer. *J. Fluid Mech.* **195**, 161–173.